Self-assembling of calcium salt of the new DNA base 5-carboxylcytosine

Simona Irrera [a,b], Sergio E. Ruiz-Hernandez [c], Melania Reggente [d], Daniele Passeri [d,*], Marco Natali [d], Fabrizio Gala [d,f], Giuseppe Zollo [d], Marco Rossi [d,e], Gustavo Portalone [a,*]

[a] Department of Chemistry, SAPIENZA University of Rome, Piazzale A. Moro 5, 00185 Rome, Italy
[b] Department of Chemistry, University College London, 20 Grodon Street, WC1H0AJ London, UK [c] School of Chemistry, Cardiff University Main Building, Park Place, CF103AT Cardiff, UK
[d] Department of Basic and Applied Sciences for Engineering, SAPIENZA University of Rome, Via A. Scarpa 16, 00161 Rome, Italy
[e] Research Center for Nanotechnology applied to Engineering of SAPIENZA University of Rome (CNIS), Piazzale A. Moro 5, 00185 Rome, Italy
[f] Department of Medical-Surgical, Techno-Biomedical Sciences and Translational Medicine of SAPIENZA University of Rome, Sant'Andrea Hospital, Rome, Italy

article info

Keywords:
Nanomedicine 5-Carboxylcytosine
Atomic force microscopy (AFM) X-ray diffraction (XRD)
Ab initio calculation
Molecular dynamics

abstract

Supramolecular architectures involving DNA bases can have a strong impact in several fields such as nanomedicine and nanodevice manufacturing. To date, in addition to the four canonical nucleobases (adenine, thymine, guanine and cytosine), four other forms of cytosine modified at the 5 position have been identified in DNA. Among these four new cytosine derivatives, 5-carboxylcytosine has been recently discovered in mammalian stem cell DNA, and proposed as the final product of the oxidative epigenetic demethylation pathway on the 5 position of cytosine. In this work, a calcium salt of 5-carboxylcytosine has been synthesized and deposited on graphite surface, where it forms self-assembled features as long range monolayers and up to one micron long filaments. These structures have been analyzed in details combining different theoretical and experimental approaches: X-ray single-crystal diffraction data were used to simulate the molecule-graphite interaction, first using molecular dynamics and then refining the results using density functional theory (DFT); finally, data obtained with DFT were used to rationalize atomic force microscopy (AFM) results.

1. Introduction

Supramolecular chemistry is based on intermolecular non-covalent interactions which include hydrogen bonds, – stacking, electrostatic, hydrophobic and charge-transfer interactions as well as metal ion coordination which cooperatively stabilize the overall structure organization. In the 3D solid state, crystal engineer-ing enables chemists to design materials with desired properties through controlled molecular self-assembly processes [1,2] and transfer, upon adsorption, determined molecular functions onto a 2D surface [3]. However, although surface-based supramolecular chemistry has received increasing interest in recent years, there remains a need to investigate the organization of molecules on surfaces into predictable architectures [4,5]. Indeed, self-assembly happens spontaneously and follows a twist of several processes involving interactions among molecules and the adsorption sur-face. Concerning organic and biological systems, the complexity of these systems result in an uncountable ensemble of possibili-ties, which could be consequently exploited in a large variety of applications [6–11]. In this context, there is no doubt about the importance of investigation of nucleobases and their derivatives. Knowledge and artificial control of DNA base pairings is extremely useful to design nanostructures by directing the base sequences at the nanoscale in a predetermined manner [10–17]. Moreover, self-assembly of nucleobases on surfaces can be potentially involved in the catalytic processes happening on mineral surfaces which are at the base of the origin of life. Indeed, RNA-like polymers might have formed by the assembly of nucleobases or similar compounds existing on Earth at the early stage of evolution [18,19].

Supramolecules in nature make use of a limited number of build-ing blocks which, in the case of DNA, are adenine (A), cytosine (C), guanine (G) and thymine (T). These four canonical nucleobases are known to pair as AT and GC holding together two complementary anti-parallel strands of DNA into a double helix [20]. Further-more, different artificial base pairs by use of various noncovalent

* Corresponding authors.
E-mail addresses: daniele.passeri@uniroma1.it (D. Passeri), gustavo.portalone@uniroma1.it (G. Portalone).

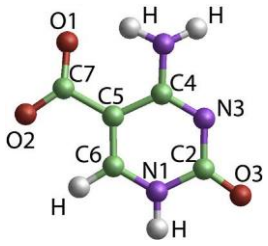

Fig. 1. The 5-carboxylcytosinate anion (caC^-) with atom labeling scheme.

interactions have been reported [21–23]. To date, four other forms of C modified at position 5 have been identified in mammalian cells [24]: 5-methylcytosine (mC); 5-hydroxymethylcytosine (hmC); 5-formylcytosine (fC); and 5-carboxylcytosine (caC) [25–27]. mC and hmC play crucial role in epigenetic regulation of gene expres-sion and maintenance of cellular identity. In fC and caC functional effects on the process of transcription remain not fully understood [28–33], although a recent study suggests caC can act as a DNA lesion [34].

AFM has been proven to have the strong capability needed to resolve nano-objects and, therefore, has been extensively used on high-resolution imaging of biological molecules [35–38]. In the case of cytosine, the AFM study of the complex process of self-assembly of cytosine on natural zeolite heulandite (010) surface shows that the adsorbed cytosine molecules form a well-ordered two-dimensional sixfold array on the surface, with the rhombic unit cell dimension being 0.58 nm, and that cytosine molecules are tilted from the surface normal of about 40° [35]. To the best of our knowledge, there are no surface studies on salts of cytosine and its derivatives with calcium ions in the literature. This is rather surprising as, among noncovalent inter-actions, metal-coordination bonding has been extensively used to design biomolecule-like supramolecular nanostructures which may potentially show magnetic and conductive properties. In par-ticular, the divalent alkaline-earth metal ions Mg^{2+} and Ca^{2+} can be chosen for metallo-ligand interactions, as they are known to play an important role in the stabilization of B-DNA by forming salt-like complexes with negatively charged phosphate oxygens, or with the unprotonated endocyclic N3 atom and exocyclic O3 atom of cytosine [39–41].

The lack of fine structural data on the newly-discovered caC, and its derivatives with divalent alkaline-earth metal cations, prompted us to provide a detailed account of the self-assembly properties of the salt formed by 5-carboxylcytosine in its ionic form (Fig. 1) and Ca^{2+}, [$(caC)_2$ -Ca]. Highly oriented pyrolytic graphite HOPG (0001) surface, which is however representative of an interesting class of materials, i.e., graphene and graphene-based nanocomposites, was chosen as the substrate for studying the self-assembly as it is easy to model and it is atomically flat, which makes it an ideal substrate for atomic force microscopy (AFM). Noticeably, in $(caC)_2$ -Ca the oxidation of the base in the 5 position causes a competition between the carboxylic function and the other possible binding sites of the cytosine molecule for the metal-ion coordination with the caC^- ligands.

This study has been carried out via the combined approach of experimental techniques, i.e., atomic force microscopy (AFM) and X-ray diffraction (XRD), and theoretical simulation methods, i.e., density functional theory (DFT) and classical molecular dynamics (MD). In particular, XRD data were used to simulate the molecule-graphite interaction, first using MD and then refining the results using DFT. Data obtained with DFT were used to rationalize our AFM experimental results.

This work is part of our continuing interest on designing of supramolecular assemblies of cytosine and its substituted deriva-tives [42–45].

2. Materials and methods

2.1. Atomic force microscopy

A portion of the solution used to grow single crystals of $(caC)_2$ - Ca for the XRD experiments has been utilized and deposited onto a freshly cleaved surface of HOPG via drop-casting. Morphological characterization of the samples has been performed using a com-mercial AFM setup (Icon, Bruker Inc.) equipped with brand new commercial Si cantilevers (RTESP, Bruker Inc.), the radius of the tip of which being certified below 10 nm by the producer. Topography and phase images have been acquired in standard tapping mode, in air and at room conditions. Images have been analyzed using the standard tools (e.g., plane subtraction, line matching, scars correc-tion, profile extraction and analysis) featured in a AFM data analysis software.

2.2. X-ray diffraction

caC (ABCR, 95% purity, $C_5H_5N_3O_3$: calcd. C 38.72, H 3.25, N 27.09; found C 37.05, H 3.36, N 26.31) has been purified by successive sub-limation under reduced pressure and suspended (0.1 mmol) in hot water (8 mL). Water solution of calcium hydroxide (Sigma Aldrich, 99.99% purity) has been then added dropwise to the suspension until pH ~8. The resulting solution has been stirred at 70 ° C for 18 h under reflux, and then filtered. Very few colorless single crystals of suitable size have been obtained from the slow room-temperature evaporation of the solution over the course of two weeks and used for X-ray diffraction experiments.

The intensity data have been collected on the Oxford Diffrac-tion Xcalibur S CCD diffractometer with graphite-monochromated Mo K_α radiation (= 0.71069 Å) at 298 (2) K operated at 50 kV and 40 mA. The data reductions have been performed using the CrysAlis software package [46]. Solution, refinement and analysis of the structure have been done using the programs integrated in the WinGX system [47]. The crystal structure has been solved by direct methods using SIR2002 [48] and refined by the full-matrix least-squares method based on F^2 using SHELXL-97 [49]. All non-hydrogen atoms have been refined anisotropically till convergence was reached. All the hydrogen atoms have been located in a dif-ference Fourier map and refined isotropically, with the exception of those hydrogen atoms linked to the C-ring atoms, which have been placed in calculated positions (C–H = 0.97 Å, U_{iso} values equal to 1.2 U_{eq} C-ring) and allowed to ride on their carrier atoms. Geo-metrical calculations have been performed using PLATON [50]. The figures have been prepared using ORTEP3 [51]. Crystals data and details of the refinement of the $(caC)_2$ -Ca structure are summarized in Table 1.

2.3. Molecular dynamics calculations

Classical molecular dynamics simulations (MD) have been employed to study the salt formation and the way it affects the caC deposition onto the (0001) HOPG surface. Due to the limita-tions inherent this techniques related mainly to transferability of the force fields and accessibility of long time scale phenomena, these simulations have been employed basically to get informa-tion on the way the eventual interactions between the caC^- and Ca^{2+} ions, both present in the deposition solution, may affect the deposition features. In the present case, indeed, water is expected to play an important role because the deposition occurs from the solution. However the expected time scale of the salt formation

Table 1
Selected crystallographic data for $(caC)_2$ -Ca heptahydrate.

Crystal data	
Chemical formula	$C_{10}H_8CaN_6O_6 \cdot 7(H_2O)$
M_r	474.42
Crystal system	Monoclinic
Space group	$P2_1/n$
Temperature (K)	298
a, b, c (A)	7.6680 (5), 16.8939 (10), 14.5101 (11)
( )	97.886 (7)
V (A)	1861.9 (2)
Z	4
Radiation type	Mo K_α
(mm^{-1})	0.42
Crystal size (mm)	0.15 × 0.12 × 0.10
Data collection	
Diffractometer	Xcalibur, Sapphire3 diffractometer
Measured reflections	30141
Independent reflections	6151
Observed reflections [I > 2 (I)]	4707
R_{int}	0.049
(sin /)max (A^{-1})	0.735
Refinement	
R[$F^2 > 2\ (F^2)$]	0.045
wR(F^2)	0.100
S	1.043
No. of parameters	351
Completeness	0.991
max ,min (e A^{-3})	0.40, −0.35
Deposit number CCDC	1015302

in water solution makes difficult, from the computational point of view, the observation of such process because Ca^{2+} ions are strongly solvated. On the other hand, the transferability limits of the force field make doubtful the predictions concerning, for instance, the hydration pattern of inorganic substrates such as HOPG. As a consequence, MD simulations have been performed without the water solvent and, therefore, should not be considered as conclu-sive but just as a way of getting preliminary general indications on the salt formation and the way the salt may affect the adsorp-tion configuration on the substrate. Nevertheless no assumptions are made about the processes or mechanism to be investigated – there is nearly no information on the configuration of molecules on the surface – and the availability of reliable force fields like AMBER allows the method to provide detailed atomic-level infor-mation that can be compared with the experiment. A more accurate calculation would request more detailed information on the pos-sible configuration of the organic overlayer. MD trajectories were calculated using the DL POLY 2 code [52]. All surface simulations have been performed at constant volume (cell parameters obtained from constant pressure calculations in the bulk) and temperature (300 K), using the Nosé-Hoover algorithm [53,54] for the thermo-stat with a relaxation time of 0.5 ps. The integration of the equations of motion has been performed using the Verlet leap-frog scheme [55]. Shake algorithm has been also employed to constrain intra-molecular hydrogen bonds. The total simulation time for each job is 1.6 ns, including 100 ps of equilibration. The convergence of the results with respect to all the precision parameters and the stabil-ity of the system evolution during the equilibrium phase have been carefully tested.

Following conventional MD simulation procedures, the system has been described by a simulation cell with three-dimensional periodic boundary conditions, wherein it contained a slab of graphite with a surface on either side. The thickness of the slab is 49.22 A, and the slab is separated by a vacuum gap of approxi-mately 28 A from its images in the next cell. 35 5-carboxycitosinate ions (caC^-) were placed in the gap on top of the surface, and one Ca^{2+} cation placed as far from the organic as possible. We used the generalized AMBER Parm99 force field for the 35 molecules, graphite surface and for non-bonded molecule-surface interac-tions. AMBER force field is an established parameter set optimized specifically for biomolecules and organic molecules, in which bond lengths and angles are described by harmonic potentials, dihedral angles by sinusoidal potentials, and non-bonded interactions by Lennard–Jones potentials. Intramolecular 1–4 (and greater) elec-trostatic and van der Waals interactions are non-zero and are unscaled. AMBER force field has been used recently to successfully study graphene organic frameworks [56]. Furthermore adsorption of amino acids and other electron acceptors on graphite [57,58] or graphene surfaces have been also carried out showing good agreement with high accuracy calculations at DFTB-D level [59]. Since the purpose of calculations is to shed light on the interac-tions molecules-surface, the graphite surface has been kept frozen, allowing the organic molecules and the ion to move and evolve freely during the simulation time.

The adsorption energy E_{ads} of the biological moiety onto the (0001) surface has been calculated as usual making use of the aver-age energy of the system measured during the MD run after the equilibration.

2.4. Ab initio calculations

The zero temperature ground state geometry of the $(caC)_2$ - Ca salt and of its adhesion properties on a HOPG surface have been obtained by ab initio total energy calculations based on the density functional theory [60,61] (DFT), with a generalized gradi-ent approximation based on the Perdew–Burke–Ernzerhof formula [62] (PBE) for the electron exchange and correlation potential $V_{XC}[n(\mathbf{r})]$ and norm-conserving pseudopotentials suitable for Ca-C interactions [63], constructed with the Troullier–Martins scheme [64] in the framework of a plane-wave basis set expansion. DFT calculations have been performed using the QUANTUM-ESPRESSO package [65], with a plane-wave energy cutoff of 70 Ry for the wave functions. Single $(caC)_2$ -Ca adsorption has been obtained starting from the XRD crystallographic data reported in Table 1 for the hydrated molecule, while the xy pyrolytic graphite surface has been modelled with a slab geometry made of two 14.77 × 12.79 A^2 graphene sheets with periodic boundary conditions (PBCs), in a vacuum region of ~35.0 A thick in the z direction, together with a dipole correction rectifying the artificial electric field across the slab induced by the PBCs [66] in the z direction. In between the hydrated $(caC)_2$ -Ca molecule and HOPG surface, a few water molecules (cor-responding to a density equal to H_2O 0.47 g/cm^3) have been added, to check explicitly the influence of hydration of the sur-face upon adsorption. Structural optimization has been achieved using the Broyden–Fletcher–Goldfarb–Shanno (BFGS) method [67] together with the Hellmann–Feynman forces acting on the ions; an empirical dispersion force term [68] has been included to handle the long range interactions (stacking). This scheme was previ-ously demonstrated to be accurate enough for cases in which van der Waals interactions among molecules are expected to play a role [69] [70]. The calculations have been performed with a 3 × 5 ×1 Monkhorst–Pack (MK) [71] k-points grid for the Brillouin zone sampling, and the ionic minimization has been done until the con-vergence threshold of 0.001 a.u. for the total force has been reached. Due to the charged state of the Ca^{2+} ion, the adsorption energy of the system has been evaluated introducing a CO_3^{2-} counter-ion in the vacuum region forcing the overall charge neutrality of the supercell [72] as:

$$E_{ads} = E_T - E_{HOPG} - E_{(caC)_2\text{-}Ca} - E_{CI} \quad (1)$$

where $E_{(caC)_2\text{-}Ca}$ and E_{CI} are the total energies of the isolated hydrated $(caC)_2$ -Ca molecule and the corresponding counter-ion,

E_T is the total energy of the system and E_{HOPG} is the energy of the hydrated HOPG surface. Young's modulus E of the periodically

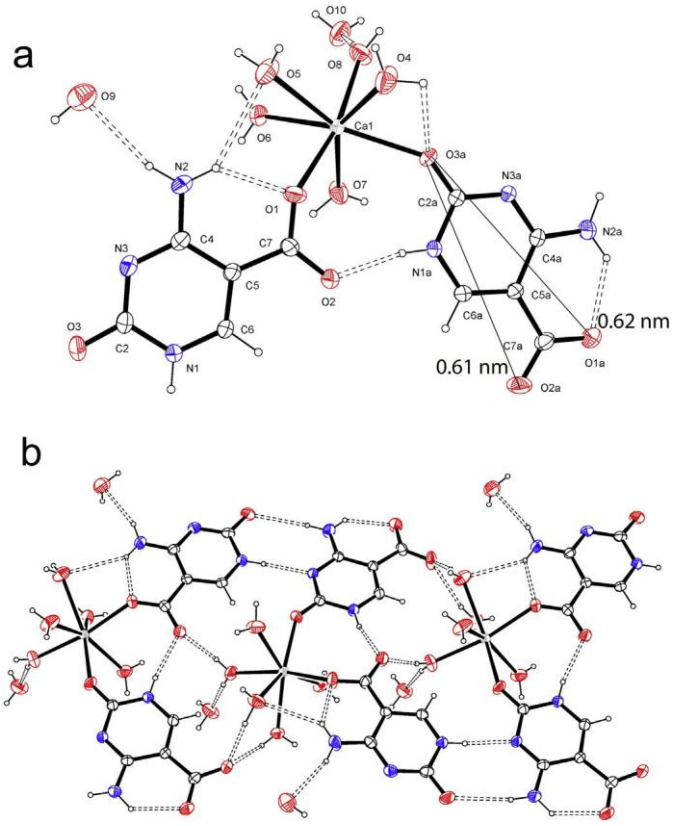

Fig. 2. XRD structure. (a) The asymmetric unit of [(caC)$_2$ -Ca], showing the atom labeling scheme and hydrogen bonding (double dashed lines). Displacements ellip-soids are drawn at 50% probability level and H atoms as small spheres of arbitrary size. Hydrogen bonds are indicated by double dashed lines. The longer dimensions of the ligand are evidenced. (b) View of the three-dimensional hydrogen-bond net-work of [(caC)$_2$ -Ca]. Displacements ellipsoids are drawn at 50% probability level and H atoms as small spheres of arbitrary size. Hydrogen bonds are indicated by double dashed lines.

repeated (caC)$_2$ -Ca salt has been evaluated starting from the XRD crystallographic data reported in Table 1, and using the same sim-ulation scheme employed for molecule adsorption (with a 3 × 2 ×2 MK k-points grid); the E value has been obtain by expressing the atomic positions in crystal coordinated and then by statically vary-ing the lattice parameter l of a specified direction. Thus E can be computed since:

$$E = \quad = F \quad l \quad = \partial l \quad l \qquad (l)^2 \quad 2 = V_0 \quad (V)^2 \qquad (2)$$

where l_0 is the equilibrium value of the lattice parameter and the cross section area. Since the total energy of the system is expected to be a quadratic function of l, i.e., $E_T = a(l)^2 = {}^{a}{}_2 (V)^2$, Eq. (2) can be recast as $E = al_0 /$. All the above described simulation parameters have been checked for convergence.

3. Results and discussion

3.1. Crystal structure analysis

(caC)$_2$ -Ca (Fig. 2a) crystallizes in the monoclinic P21/n space group. The asymmetric unit contains one Ca^{2+} ion in pentagonal-bipyramidal geometry, two caC^{-} ligands and seven water molecules (Fig. 2a). In the crystal, the two ligands are present as pla-nar aminooxo tautomers deprotonated at the carboxyl group. The pattern of bond lengths and bond angles of the caC^{-} ions agrees with that reported in previous structural investigations [73]. The Ca^{2+} ion is seven-coordinated in pentagonal-bipyramidal geome-try, and the Ca-O bond lengths are in the range 2.307 (1)–2.506 (1) Å. Ca^{2+} is coordinated in the basal plane by one O atom of the C═O of one caC^{-} ligand and four water molecules. The two axial positions are then occupied by one O atom of the carboxylate moiety and one of the three remaining water molecules. Therefore, in (caC)$_2$ - Ca the carboxylic function represents an additional binding site for the metal-ion coordination with respect to the unsubstituted cyto-sine molecule [74]. A similar pentagonal-bipyramidal coordination geometry has been reported in crystals of cytosine-calcium chlo-ride (1:1) complex [74]. Indeed, in this crystal structure, the Ca^{2+} ion is coordinated in the basal plane by two Cl^{-} ions related by the c-glide symmetry, the endocyclic N3 atom and exocyclic O3 atom of a cytosine base, and the O3 atom of an adjacent cytosine base. The two axial positions are occupied by a Cl^{-} ion and a water molecule. In (caC)$_2$ -Ca, the observed competition between the two binding sites in the ligand is not surprising, and it has been addressed by several studies in similar compounds [75].

The mutual arrangement of the different fragments in the unit cell gives rise to a layered structure strengthened by non-covalent interactions which form a complex 3D network of hydrogen bonds (Fig. 2b). From XRD results, the maximum length of 0.61–0.62 nm has been estimated for the single ligand (Fig. 2a).

3.2. Analysis of self-assembled superstructures: monolayer

AFM imaging of (caC)$_2$ -Ca deposited on a flat HOPG (0001) surface reveals, in different areas of the drop, large formations with width of some microns and height ranging from some nanometers to some tens of nanometers (images not shown), which are likely to be disordered agglomerates of molecules and are not further investigated in this work. Conversely, far from these agglomerates, AFM images show the presence of a self-assembled film, almost continuous on areas a few microns wide although several inter-ruptions are visible. As an example, Fig. 3a shows a 1 × 1 m^2 of the deposited surface revealing the presence of an almost uniform long range film, onto which several filaments with length of several hundred of nanometers can be observed. Interruptions in the layer leave small areas free from the molecules coverage (a detail is reported in Fig. 3b). In the corresponding phase image (Fig. 3c), the (caC)$_2$ -Ca layer is characterized by a phase shift different from that of the underlying material which therefore can be rationalized as the HOPG substrate instead of another (caC)$_2$ -Ca layer. In addition, in correspondence of the (caC)$_2$ -Ca layer a phase shift is detected which is more positive than that of the HOPG substrate. This indicates that the molecular layer is 'stiffer' than the HOPG substrate or, more precisely, that energy dissipation during a cycle of tapping is smaller in correspondence of the monolayer than in correspondence of the HOPG substrate [76]. Taking advantage of the unveiled HOPG region, the thickness of the layer can be deduced from a section of the topography along a horizontal line, i.e., the 'fast scan' direction in the reported AFM image, such as that reported in Fig. 3d. The thickness of the layer is measured as high as 0.8 ± 0.1 nm, which suggests that it is actually a monolayer covering almost uniformly the surface of the HOPG substrate. This thickness, however, is slightly larger than the expected maxi-mum length of the molecule determined by XRD (0.61–0.62 nm). Moreover, taking advantage of the presence of the different discon-tinuities in the layer in Fig. 3a, we evaluated the thickness of the layer in different points on the same portion of surface obtaining a thickness varying in the range 0.8–1.1 nm, with an average value of 0.91 ± 0.14 nm. In addition, differences as high as a few tenths of angstrom can be obtained on the same profile depending on the subtraction of a first or second order surface (which are standard procedures in AFM image analysis) to the image. Therefore, to

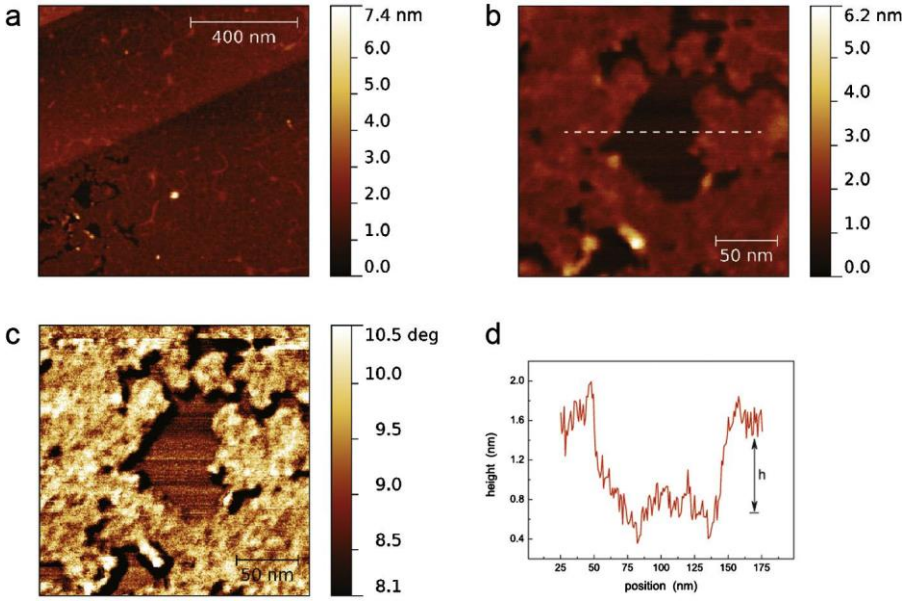

Fig. 3. AFM characterization of $(caC)_2$ -Ca superstructures self-assembled on HOPG. (a) Topography of a 1 × 1 m^2 area indicating that the surface is covered by a molecular monolayer on which some filaments are present. (b) Closer view of the topography showing discontinuities in the monolayer which reveal the HOPG substrate. (c) Corre-sponding phase imaging evidencing that the layer and exposed substrate are constituted by different materials. (d) Profile extracted in correspondence of the line shown in the inset from which the thickness of the layer is evaluated as 0.8 ± 0.1 nm, compatible with a single-molecule layer.

confirm that the observed layer is really a monolayer and to rationalize the variability of the thickness even in sub-micrometer scales, we carried out MD and DFT simulations to analyze the interaction between the $(caC)_2$ -Ca molecule and a HOPG (0001) surface and to predict its 'apparent' height as measured by AFM.

Our first attempt to explain the observed experimental features consisted in MD simulations of several caC^- molecules on HOPG to provide information on the molecule-surface interaction either in presence of the Ca^{2+} ion or not. The approach followed here is not intended to be exhaustive, as we have not considered the effects due to surface hydration and water molecules coordinated by Ca^{2+} . Indeed, HOPG is simulated bare whereas it is known to be hydrated as the AFM measurements are conducted in air [77]. Even in the above limits, several interesting features emerged from MD, especially concerning the caC^- orientation and the tendency to form the $(caC)_2$ -Ca salt in the solution deposited onto the HOPG surface. In particular, we have simulated the system described in Section 2.3 either with or without a Ca^{2+} ion to put in evidence

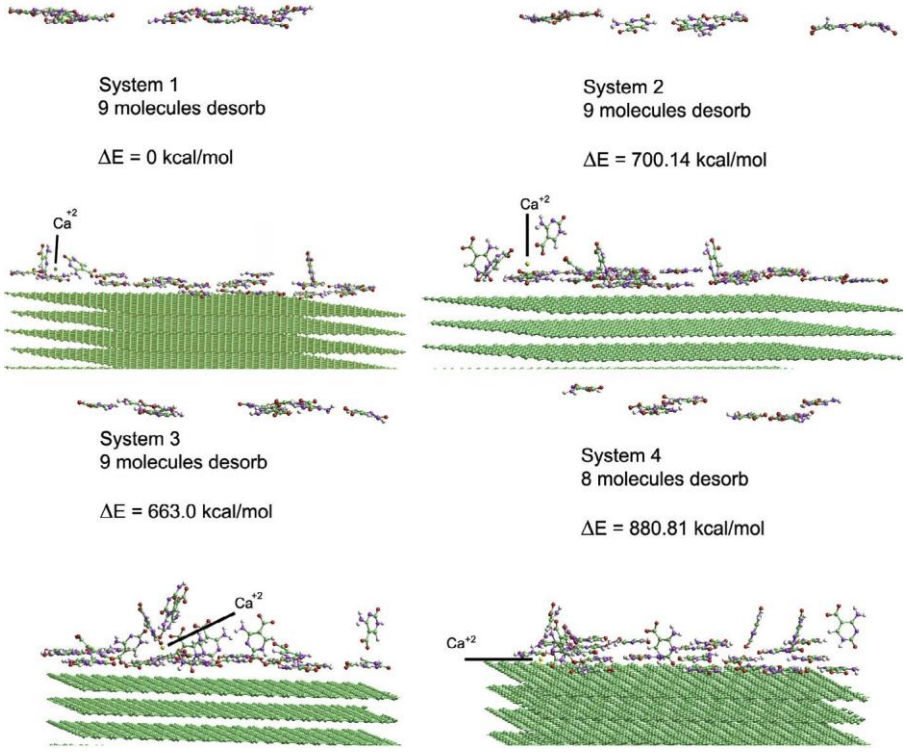

Fig. 4. The four final configurations resulting from the MD are presented. System 1 is the most stable one. Calcium ion is highlighted.

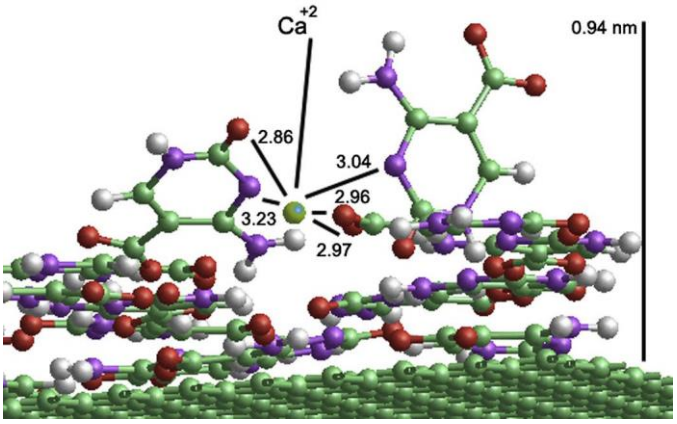

Fig. 5. The chemical environment of calcium ion which coordinates three caC^{-}. We evidenced the coordination bond lengths and the calculated height of this aggregate. All bond distances are in angstrom. The highest point in the adlayer is equal to 0.94 nm.

the salt formation and the possible adsorption features that cannot be ascribed to caC^{-} only. Our approach consisted in designing six systems with different initial coordinates: three with 35 horizon-tal caC^{-} molecules (systems 1, 3 and 5) and three with 35 vertical molecules (systems 2, 4 and 6); for both the horizontal and vertical caC^{-} initial coordinates, we have considered three cases: the pres-ence of one Ca^{2+} ion initially close to the HOPG substrate (systems 3 and 4), the presence of one Ca^{2+} ion initially far from the HOPG substrate (systems 1 and 2) and no Ca^{2+} in the supercell (systems 5 and 6).

A complex scenario emerged from the MD simulations of the above systems, some of the typical configurations found being pre-sented in Figs. 4 and 5. We could observe that ~75% of the molecules stay on the surface (with 8–9 molecules desorbing from it) and show different adsorption configurations with nearly ~60–90% of them forming horizontal adhesion geometry, nearly ~7–8% being vertically aligned and the remaining molecules (~33–2%) forming complex structures around the calcium ion. Some general features can be outlined: first, horizontal adhesion of caC^{-} molecules pre-vails independently on the starting configuration, either horizontal or vertical; second, the Ca^{2+} ion always interacts with the adlayer and never interacts with the substrate; third, the equilibrium adsorption configurations is rapidly reached (after about 300 ps) and stays quite stable during the remaining simulation time. More importantly, among the equilibrium configurations detected (see Fig. 4), the most stable one (system 1 in Fig. 4) shows the most marked horizontal arrangement of the CaC^{-} ligands around the Ca^{2+}. Configuration 5 and 6 cannot be compared energetically as they miss calcium ion in the slab.

In Fig. 5, details of the aggregate in system 1 are shown. First of all it must be underlined that the absence of water solvent in the simulation induces an over-coordination of the Ca^{2+} ion with three caC^{-} molecules via two N-ring, one carbonyl oxygen and two carboxyl oxygens; this scenario differs from the one emerged from the XRD of the $(caC)_2$ -Ca salt where five water molecules basically replace the caC^{-} that is vertically coordinated to the Ca^{2+} ion. More-over, the Ca–O bond lengths are overestimated by about 15% with respect to the ones measured in XRD due to transferability lim-its of the Ca–O model potential included in AMBER [78]. Lastly, due to the presence of just one Ca^{2+}, several uncoordinated caC^{-} molecules seem to form the first adsorption layer, just below the salt, onto the HOPG substrate. In any case, MD simulations show very clearly that the salt is easily formed and that the horizontal adsorption geometry is the most stable one. However, the limits of the MD model require a more accurate modelling of the adsorption configurations that must explicitly consider the presence of water molecules both in the salt and on the HOPG surface.

Then, following the first indications obtained from MD, a more reliable insight on the atomic arrangement of the adsorption con-figuration has been obtained by studying, in the context of DFT total energy calculations at zero temperature, the horizontal adsorption of a fully hydrated $(caC)_2$ -Ca single monolayer film (using the initial coordinates obtained from XRD) on a hydrated HOPG surface; the corresponding ground state adsorption configuration is reported in Fig. 6, from which some important features can be inferred. In the ground state structure the Ca^{2+} ion is seven coordinated, with Ca–O bond lengths ranging from 2.34 Å to 2.50 Å, in very good agree-ment with the XRD data previously reported. Next, the equilibrium distance between the surface and the $(caC)_2$ -Ca monolayer d was evaluated. If one considers the distance between the graphite and the Ca atom, the molecule thickness results to be 0.76 nm (Fig. 6), which reaches 0.97 nm or 1.06 nm if one starts from the O or the H atom of the uppermost water molecule bounded to the Ca^{2+} ion. The actual height measured with AFM depends on the interac-tion force between the tip and the molecule, in particular on the

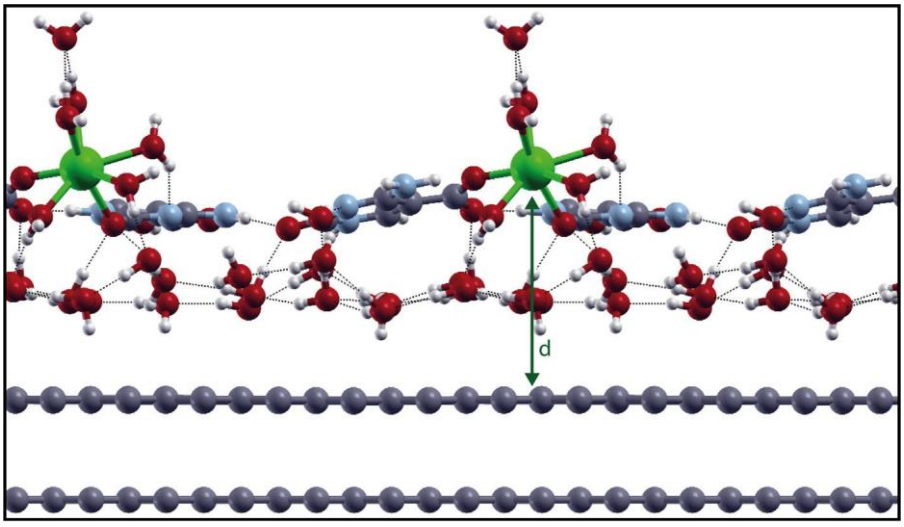

Fig. 6. (Zero temperature ground state configuration of a hydrated $(caC)_2$ -Ca single monolayer film adsorbed on a HOPG surface as predicted by DFT calculations. The black dotted lines in the figure show the hydrogen bond network between H_2O molecules in-between the surface and the self-assembled monolayer.

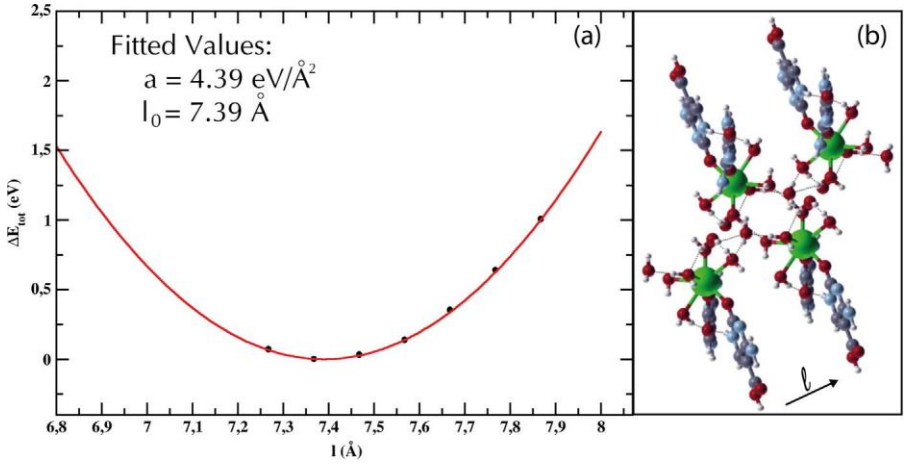

Fig. 7. (Total energy variation of the hydrated (caC)2 -Ca salt as a function of the relative displacement l in (a), while in (b) the deformation direction l is specified with respect the ground state structure obtained after DFT structural optimization of the XRD data.

possible deformation of the water molecules bounded to the Ca^{2+} ion. In addition, a possible source of discrepancy between DFT and AFM experiments can be due to the fact that DFT is performed at a temperature of 0 K. The rationalization of this issue requires further detailed studies, to understand the possible deformation of the molecules under AFM tapping, which are currently ongo-ing. Overall, the expected height of a single monolayer does range between 0.8 nm and 1 nm which is in good agreement with AFM data. In any case, the measured thickness is significantly smaller than that one would expect in the case of a bilayer. Therefore, we can confirm that, at least on relatively small areas free from bigger agglomerates of material, we are in presence of a self-assembled monolayer. Moreover, the water layer between the HOPG sur-face and the (caC)2 -Ca film forms a hydrogen bond network that might help in stabilizing self-assembling forming an intermolecu-lar H-bonds network between NH_2 and CO groups of adjacent caC molecules. Then, the present DFT results strongly support the inter-pretation of the AFM measurements in terms of a single (caC)2 -Ca salt monolayer deposited onto the HOPG surface. However, a ques-tion arises on the possible mismatch between AFM data and the numerical simulations carried out, due to the different elasticity between the (caC)2 -Ca monolayer and the HOPG substrate, as well as to the small thickness of the layer [79]. Indeed, it is well known that variations in the sample topography produce artifacts in AFM mapping of sample physical properties, e.g., mechanical [80] or magnetic [81,82]. If such mismatch occurred, then the agreement between the AFM and the numerical data would be just fictitious. It should be also noted, however, that systematic errors in the evalua-tion of height and thus artifacts in topography images are produced by non homogeneous physical properties on the sample surface. For example, variations of elastic modulus produce height anomalies in AFM topographies [83–87] as well as variation of electric proper-ties produces height anomalies in scanning tunneling microscopy (STM) topographies [88]. To address such issue and to dispel the above doubts, the Young's modulus E of the (caC)2 -Ca salt must be evaluated. The sub-nanometer thickness of the layer prevents the easy determination of the elastic modulus of the layer from the measured value for the layer-substrate system, both using methods based on quasi-static [89] or dynamic indentation with AFM [90]. Recently, this challenging task has been addressed using contact resonance AFM (CR-AFM), which has been proven to be sensitive to stiffness variations arisen from even a single atomic layer of a van der Waals-adhered materials [91]. In this work, for the sake of sim-plicity, E of the (caC)2 -Ca salt has been computed through Eq. (2); in Fig. 7a the resulting total energy profile variation is reported for a deformation of the crystal structure along the l direction (sketched in Fig. 7b together with the equilibrium configuration obtained for the(caC)2 -Ca salt), almost (anti-)parallel to the orthogonal direc-tion of the HOPG surface in Fig. 6. The obtained energy profile is almost quadratic, as expected, from which a Young's modulus of E 21 GPa is obtained. The fitted equilibrium value for l_0 is 7.4 Å, lower than the one obtained from XRD data of 7.67 Å. This is not sur-prising since XRD experimental data have been collected at room temperature (see Table 1), while DFT simulations have been car-ried out at T = 0 K. The order of magnitude of the calculated value of Young's modulus, significantly larger than that observed in soft matter like polymers [89,92,93], can be justified by considering that in similar molecules the presence of aromatic rings is responsible for modulus values as high as 100 GPa [94,95]. The Young's mod-ulus of HOPG substrate is close to that of the molecule. Recently, indeed, Eskelsen at al. [96] reported values of about 25 GPa, com-patible with the nominal value of 18 GPa, although values as high as 30 GPa [97,98] or as low as 10 GPa [99] have also been reported. The error in the determination of the height can be evaluated fol-lowing the approach reported by Santos et al. [79]. Assuming an average value of 20 GPa for HOPG Young's modulus does not lead to any significant anomaly in the height, while assuming the values of 10 GPa or 30 GPa leads to an overestimation or underestimation, respectively, of the monolayer on HOPG as small as 0.2 Å, negligible with respect the uncertainty in the AFM results.

3.3. Analysis of self-assembled superstructures: filaments

As already mentioned, several filaments were observed ran-domly distributed on the surface of the monolayer (Figs. 3 and 8). These filaments have been extensively found on the surface with length up to 1 m. The profiles of the filaments shown in Fig. 8d emphasize the height of these structures where z section ranges from 0.7 ± 0.2 nm to 1.0 ± 0.2 nm. The relatively large uncertainty in the determination of the height values arises from the roughness of the underlying monolayer on which the filaments are deposited. Following the procedure reported by Santos et al. [79], we could assess the negligibility of the error in the estimation of the height of a single molecule on a molecule monolayer. Overall, our results are compatible with single-molecule structure physisorbed on the underlying monolayer. A possible explanation in the formation of such filaments lies in the non-covalent, dipolar bonds arising between single molecules. Due to the presence of the electron lone pairs coming from N and O atoms interacting with polar amino (NH_2) and hydroxyl (OH) groups [100], in fact, such long-range

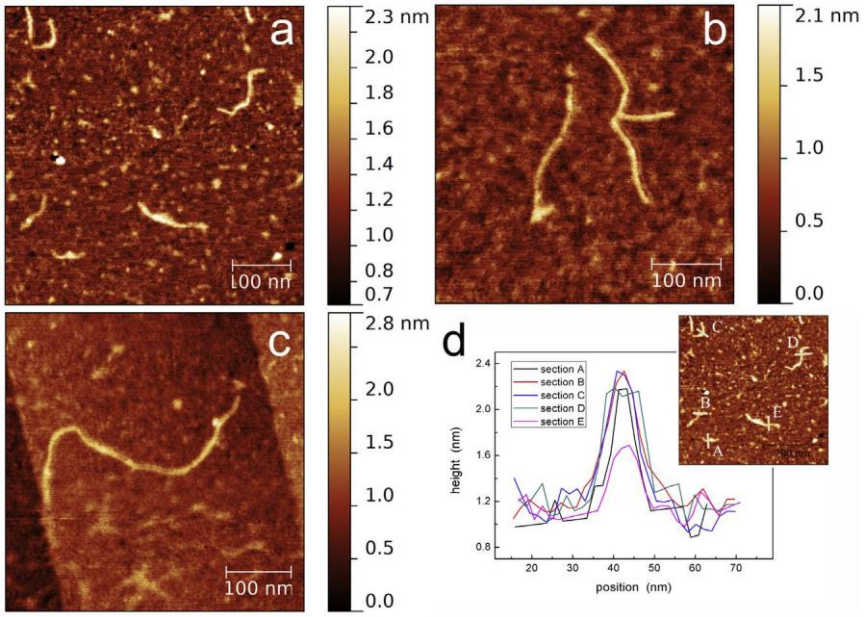

Fig. 8. AFM characterization of self-assembled filaments on the monolayer. (a) Portion of the surface where some filaments are visible. (b) Two filaments, one of which is bifurcated the height of which is 1.0 ± 0.2 nm, while the other one is 0.7 ± 0.1 nm high. (c) Filament grown between two edges of the HOPG substrate with height of 1.0 ± 0.2 nm. (d) Profiles of the main five filaments having height in the range 0.7–1.0 nm.

interactions may, in principle, favor the formation of H bonds link-ing different planar molecules in long filaments.

4. Conclusions

In this work, we have performed a combined approach that includes AFM, XRD and MD and ab initio calculations to investigate the deposition of $(caC)_2$ -Ca salt on HOPG. Although the accuracy of AFM could be increased by the use of the ultra high vacuum and temperature control equipment, and MD could have been limited by the paucity of initial information and surface hydration, our results clearly show a self-assembly giving rise to long-range monolayers as well as filaments whose length has been observed up to 1 m. The structural information obtained from XRD of the deposited compound has allowed us to accurately estimate the length of a single molecule (0.61–0.62 nm) and to compare it with the z-section measured with AFM imaging. This comparison provides insight in the self-assembled entities found on the sur-face. According to the combined results obtained from AFM, MD and total energy ab initio calculations, long range adsorption fea-tures observed and measured by AFM are interpreted as a single monolayer of self-assembled $(caC)_2$ -Ca salt deposited from water solution onto the HOPG substrate. Moreover, DFT results support such interpretation on the basis of comparable elastic properties of the salt and the substrate. In this work, we presented inter-esting structures – monolayers and filaments – produced by the self-assembling of $(caC)_2$ -Ca on a particular substrate (HOPG). Stud-ies aiming at elucidating the experimental conditions to obtain wider and more uniform monolayers are required and are currently ongoing, as well as theoretical studies are in progress to clarify the atomistic nature of the observed features.

Author's contribution

GP performed and analyzed XRD measurements. SI and SERH carried out MD calculations. MRe and DP performed the AFM mea-surements which were analyzed by MRe, MN, DP, and MRo. MN and FG carried out numerical analysis of height artifacts in AFM images. FG and GZ performed DFT calculations. The manuscript was written through contributions of all authors. All authors have given approval to the final version of the manuscript.

Funding sources

SI was supported by the Newton International Alumni Schemes of the Royal Society.

Conflict of interests

The authors declare no competing financial interests.

Acknowledgments

The authors acknowledge the use of the UCL Legion High Performance Computing facility, and associated services, in the completion of this work. SI and SERH acknowledge N. De Leeuw and D. Di Tommaso for the essential discussions. Computa-tional resources for DFT calculations have been provided by CRESCO/ENEAGRID High Performance Computing infrastructure and its staff [101]. CRESCO/ENEAGRID High Performance Comput-ing infrastructure is funded by ENEA, the Italian National Agency for New Technologies, Energy and Sustainable Economic Develop-ment and by Italian and European research programmes, see http://www.cresco.enea.it/english for information.

References

[1] J.-M. Lehn (Ed.), Supramolecular Chemistry: Concepts and Perspectives, Wiley-VCH Verlag GmbH & Co, KGaA, 2006.
[2] J.M. Lehn, Cryptates: inclusion complexes of macropolycyclic receptor molecules, Pure Appl. Chem. 50 (1978) 871–892.
[3] D.Y. Petrovykh, V. Pérez-Dieste, A. Opdahl, H. Kimura-Suda, J.M. Sullivan, M.J. Tarlov, F.J. Himpsel, L.J. Whitman, Nucleobase orientation and ordering in films of single-stranded DNA on gold, J. Am. Chem. Soc. 128 (2006) 2–3.
[4] N. Miyashita, D.G. Kurth, Directing supramolecular assemblies on surfaces, J. Mater. Chem. 18 (2008) 2636–2649.
[5] A.G. Slater, L.M.A. Perdigão, P.H. Beton, N.R. Champness, Surface-based supramolecular chemistry using hydrogen bonds, Acc. Chem. Res. 47 (12) (2014) 3417–3427.

[6] S. Barlow, R. Raval, Nanoscale insights in the creation and transfer of chirality in amino acid monolayers at defined metal surfaces, Curr. Opin. Colloid Interface Sci. 13 (2008) 65–73.
[7] S. Irrera, D. Costa, New insight brought by density functional theory on the chemical state of alaninol on Cu(100): energetics and interpretation of X-ray photoelectron spectroscopy data, J. Chem. Phys. 128 (2008) 114709.
[8] S. Irrera, G. Contini, N. Zema, S. Turchini, J. Fujii, S. Sanna, T. Prosperi, Two-dimensional chiral single domain by d-alaninol functionalization of Cu(100), J. Phys. Chem. B 111 (2007) 7478–7480.
[9] S. Irrera, G. Contini, N. Zema, S. Turchini, S. Sanna, P. Moras, C. Crotti, T. Prosperi, Adsorption of d-alaninol on Cu(100), Surf. Sci. 601 (2007) 2562–2565.

[10] G. Portalone, M. Colapietro, F. Ramondo, L. Bencivenni, A. Pieretti, The effect of hydrogen bonding on the structures of uracil and some methyl derivatives by experiment and theory, Acta Chem. Scand. 53 (1999) 57–68.
[11] M. Habgood, S.L. Price, G. Portalone, S. Irrera, Testing a variety of electronic-structure-based methods for the relative energies of 5-formyluracil crystals, J. Chem. Theor. Comput. 7 (2011) 2685–2688.
[12] I. Bald, S. Weigelt, X. Ma, P. Xie, R. Subramani, M. Dong, C. Wang, W. Mamdouh, J. Wang, F. Besenbacher, Two-dimensional network stability of nucleobases and amino acids on graphite under ambient conditions: adenine, l-serine and l-tyrosine, Phys. Chem. Chem. Phys. 12 (2010) 3616–3621.

[13] S. Irrera, N.H. de Leeuw, A density functional theory study of the adsorption of uracil on the Au(100) surface, Proc. Royal Soc. A 467 (2011) 1959–1969.
[14] W. Mamdouh, M. Dong, S. Xu, E. Rauls, F. Besenbacher, Supramolecular nanopatterns self-assembled by adenine-thymine quartets at the liquid/solid interface, J. Am. Chem. Soc. 128 (2006) 13305–13311.
[15] S. Irrera, A. Roldan, G. Portalone, N.H. De Leeuw, The role of hydrogen bonding and proton transfer in the formation of uracil networks on the Gold (100) surface: a density functional theory approach, J. Phys. Chem. C 117 (2013) 3949–3957.

[16] S. Irrera, G. Portalone, N.H. De Leeuw, Chemisorption of uracil on gold surfaces via density functional theory, Surf. Sci. 614 (2013) 20–23.
[17] R. Duncan, Nanomedicine gets clinical, Mater. Today 8 (2005) 16–17.
[18] S.J. Sowerby, W.M. Heckl, The role of self-assembled monolayers of the purine and pyrimidine bases in the emergence of life, Orig. Life Evol. Biosph. 28 (1998) 283–310.

[19] S.J. Sowerby, P.A. Stockwell, W.M. Heckl, G.B. Petersen, Self-programmable, self-assembling two-dimensional genetic matter, Orig. Life Evol. Biosph. 30 (2000) 81–99.

[20] J.D. Watson, F.H.C. Crick, A structure for deoxyribose nucleic acid, Nature 171 (1953) 737–738.
[21] S.A. Benner, Understanding nucleic acids using synthetic chemistry, Acc. Chem. Res. 37 (2004) 784–797.
[22] G. Portalone, S. Irrera, Supramolecular structure of unnatural nucleobases: revised structure of (2:1) 6-methylisocytosinium dihydrogen monophosphate adduct, J. Mol. Struct. 991 (2011) 92–96.
[23] G. Portalone, J.O. Moilanen, H.M. Tuononen, K. Rissanen, The role of weak hydrogen bonds and halogen bonds in 5-halo-1,3-dimethyluracils and their cocrystals – a combined experimental and computational study, Cryst. Growth Des. 16 (2016) 2631–2639.
[24] R.D. Hotchkiss, The quantitative separation of purines, pyrimidines, and nucleosides by paper chromatography, J. Biol. Chem. 175 (1948) 315–332.
[25] C.S. Nabel, R.M. Kohli, Molecular biology. Demystifying DNA demethylation, Science 333 (2011) 1229–1230.
[26] S. Kriaucionis, N. Heintz, The nuclear DNA base 5-hydroxymethylcytosine is present in Purkinje neurons and the brain, Science 324 (2009) 929–930.
[27] M. Tahiliani, K.P. Koh, Y. Shen, W.A. Pastor, H. Bandukwala, Y. Brudno, S. Agarwal, L.M. Iyer, D.R. Liu, L. Aravind, A. Rao, Conversion of 5-methylcytosine to 5-hydroxymethylcytosine in mammalian DNA by MLL partner TET1, Science 324 (2009) 930–935.
[28] T. Pfaffeneder, B. Hackner, M. Truß, M. Münzel, M. Müller, C.A. Deiml, C. Hagemeier, T. Carell, The discovery of 5-formylcytosine in embryonic stem cell DNA, Angew. Chem. Int. Ed. 50 (2011) 7008–7012.
[29] S. Ito, L. Shen, Q. Dai, S.C. Wu, L.B. Collins, J.A. Swenberg, C. He, Y. Zhang, Tet proteins can convert 5-methylcytosine to 5-formylcytosine and 5-carboxylcytosine, Science 333 (2011) 1300–1303.
[30] Y.-F. He, B.-Z. Li, Z. Li, P. Liu, Y. Wang, Q. Tang, J. Ding, Y. Jia, Z. Chen, L. Li, Y. Sun, X. Li, Q. Dai, C.-X. Song, K. Zhang, C. He, G.-L. Xu, Tet-mediated formation of 5-carboxylcytosine and its excision by TDG in mammalian DNA, Science 333 (2011) 1303–1307.
[31] R. Jaenisch, A. Bird, Epigenetic regulation of gene expression: how the genome integrates intrinsic and environmental signals, Nat. Genet. 33 (2003) 245–254.

[32] J.A. Law, S.E. Jacobsen, Establishing, maintaining and modifying DNA methylation patterns in plants and animals, Nat. Rev. Genet. 11 (2010) 204–220.

[33] M. Münzel, U. Lischke, D. Stathis, T. Pfaffeneder, F.A. Gnerlich, C.A. Deiml, S.C. Koch, K. Karaghiosoff, T. Carell, Improved synthesis and mutagenicity of oligonucleotides containing 5-hydroxymethylcytosine, 5-formylcytosine and 5-carboxylcytosine, Chem. Eur. J. 17 (2011) 13782–13788.
[34] T. Shibutani, S. Ito, M. Toda, R. Kanao, L.B. Collins, M. Shibata, M. Urabe, H. Koseki, Y. Masuda, J.A. Swenberg, C. Masutani, F. Hanaoka, S. Iwai, I. Kuraoka, Guanine-5-carboxylcytosine base pairs mimic mismatches during DNA replication, Sci. Rep. 4 (2014) 5220.

[35] M. Komiyama, M. Gu, T. Shimaguchi, H.-M. Wu, T. Okada, Adlayer formation of DNA base cytosine over natural zeolite heulandite (010) surface by AFM, Appl. Phys. A 66 (1998) S635–S637.
[36] F. Kienberger, A. Ebner, H.J. Gruber, P. Hinterdorfer, Molecular recognition imaging and force spectroscopy of single biomolecules, Acc. Chem. Res. 39 (2006) 29–36.

[37] R.E.A. Kelly, L.N. Kantorovich, Planar nucleic acid base super-structures, J. Mater. Chem. 16 (2006) 1894–1905.
[38] J. Fritz, M.K. Baller, H.P. Lang, H. Rothuizen, P. Vettiger, E. Meyer, H.J. Güntherodt, C. Gerber, J.K. Gimzewski, Translating biomolecular recognition into nanomechanics, Science 288 (5464) (2000) 316–318.
[39] Z.A. Tehrani, A. Fattahi, A. Pourjavadi, Interaction of Mg^{2+} , Ca^{2+} , Zn^{2+} and Cu^{+} with cytosine nucleosides: influence of metal on sugar puckering and stability of N-glycosidic bond, a DFT study, J. Mol. Struct. – THEOCHEM 913 (1–3) (2009) 117–125.
[40] M.H. Shamsi, H.-B. Kraatz, Interactions of metal ions with DNA and some applications, J. Inorg. Organomet. Polym. Mater. 23 (1) (2013) 4–23.
[41] W. Zhou, R. Saran, P.-J.J. Huang, J. Ding, J. Liu, An exceptionally selective DNA cooperatively binding two Ca^{2+} ions, ChemBioChem 18 (2017) 1–6.
[42] G. Portalone, M. Colapietro, Redetermination of 5-fluoro-cytosine monohydrate, Acta Crystallogr. E 62 (3) (2006) o1049–o1051.
[43] G. Portalone, M. Colapietro, Asymmetric base pairing in the complex 5-fluorocytosinium chloride/5-fluorocytosine monohydrate, J. Chem. Crystallogr. 37 (2) (2007) 141–145.
[44] G. Portalone, M. Colapietro, The 1:1 complex of cytosine and 5-fluorouracil monohydrate revisited, Acta Crystallogr. C 63 (7) (2007) o423–o425.
[45] G. Portalone, M. Colapietro, Solid-phase molecular recognition of cytosine based on proton-transfer reaction, J. Chem. Crystallogr. 39 (3) (2009) 193–200.

[46] Oxford, Diffraction CrysAlis Software System, Oxford Diffraction Ltd, 2008.
[47] L.J. Farrugia, WinGX suite for small-molecule single-crystal crystallography, J. Appl. Crystallogr. 32 (1999) 837–838.
[48] M.C. Burla, M. Camalli, B. Carrozzini, G.L. Cascarano, C. Giacovazzo, G. Polidori, R. Spagna, SIR2002: the program, J. Appl. Crystallogr. 36 (2003) 1103.

[49] G.M. Sheldrick, A short history of SHELX, Acta Crystallogr. A 64 (2008) 112–122.
[50] A.L. Spek, Single-crystal structure validation with the program PLATON, J. Appl. Crystallogr. 36 (2003) 7–13.
[51] L.J. Farrugia, ORTEP-3 for Windows – a version of ORTEP-III with a Graphical User Interface (GUI), J. Appl. Crystallogr. 30 (1997) 565.
[52] W. Smith, T.R. Forester, DL_POLY 2.0: a general-purpose parallel molecular dynamics simulation package, J. Mol. Graph. 14 (1996) 136–141.
[53] S. Nosé, A unified formulation of the constant temperature molecular dynamics methods, J. Chem. Phys. 81 (1984) 511–519.
[54] W.G. Hoover, Canonical dynamics: equilibrium phase-space distributions, Phys. Rev. A 31 (1985) 1695–1697.
[55] L. Verlet, Computer "experiments" on classical fluids. I. Thermodynamical properties of Lennard–Jones molecules, Phys. Rev. 159 (1967) 98–103.
[56] A. Nicolaï, P. Zhu, B.G. Sumpter, V. Meunier, Molecular dynamics simulations of graphene oxide frameworks, J. Chem. Theory Comput. 9 (2013) 4890–4900.

[57] B.E. Owens, A. Riemann, A computational analysis for amino acid adsorption, Surf. Sci. 624 (2014) 118–129.
[58] A. Riemann, B.E. Owens, Molecular mechanics modeling of the adsorption of methionine on graphite, Surf. Sci. 604 (2010) 2084–2090.
[59] S. Haldar, M. Kolář, R. Sedlák, P. Hobza, Adsorption of organic electron acceptors on graphene-like molecules: quantum chemical and molecular mechanical study, J. Phys. Chem. C 116 (2012) 25328–25336.
[60] P. Hohenberg, W. Kohn, Inhomogeneous electron gas, Phys. Rev. 136 (1964) B864–B871.
[61] W. Kohn, L.J. Sham, Self-consistent equations including exchange and correlation effects, Phys. Rev. 140 (1965) A1133–A1138.
[62] J.P. Perdew, K. Burke, M. Ernzerhof, Generalized gradient approximation made simple, Phys. Rev. Lett. 77 (1996) 3865–3868.
[63] F. Gala, G. Zollo, Augmented methane adsorption at ca decorated carbon nanotubes – a DFT study, J. Phys. D: Appl. Phys. 47 (2014) 075305.
[64] N. Troullier, J.L. Martins, Efficient pseudopotentials for plane-wave calculations, Phys. Rev. B 43 (1991) 1993–2006.
[65] P. Giannozzi, S. Baroni, N. Bonini, M. Calandra, R. Car, C. Cavazzoni, D. Ceresoli, G.L. Chiarotti, M. Cococcioni, I. Dabo, A. Dal Corso, S. de Gironcoli, S. Fabris, G. Fratesi, R. Gebauer, U. Gerstmann, C. Gougoussis, A. Kokalj, M. Lazzeri, L. Martin-Samos, N. Marzari, F. Mauri, R. Mazzarello, S. Paolini, A. Pasquarello, L. Paulatto, C. Sbraccia, S. Scandolo, G. Sclauzero, A.P. Seitsonen, A. Smogunov, P. Umari, R.M. Wentzcovitch, QUANTUM ESPRESSO: a modular and open-source software project for quantum simulations of materials, J. Phys. Condens. Matter 21 (2009) 395502.
[66] L. Bengtsson, Dipole correction for surface supercell calculations, Phys. Rev. B 59 (1999) 12301–12304.
[67] R. Fletcher, A new approach to variable metric algorithms, Comput. J. 13 (1970) 317–322.
[68] S. Grimme, Semiempirical GGA-type density functional constructed with a long-range dispersion correction, J. Comput. Chem. 27 (2006) 1787–1799.
[69] M. Feroci, I. Chiarotto, F. D'Anna, F. Gala, R. Noto, L. Ornano, G. Zollo, A. Inesi, N-heterocyclic carbenes and parent cations: acidity, nucleophilicity,

stability, and hydrogen bonding-electrochemical study and ab initio calculations, ChemElectroChem 3 (2016) 1133–1141.
[70] F. Gala, L. Mattiello, F. Brunetti, G. Zollo, Electronic excitations in solution-processed oligothiophene small-molecules for organic solar cells, J. Chem. Phys. 144 (2016) 084310.
[71] H.J. Monkhorst, J.D. Pack, Special points for Brillouin-zone integrations, Phys. Rev. B 13 (1976) 5188–5192.
[72] L. Agosta, G. Zollo, C. Arcangeli, F. Buonocore, F. Gala, M. Celino, Water driven adsorption of amino acids on the (101) anatase TiO_2 surface: an ab initio study, Phys. Chem. Chem. Phys. 17 (2015) 1556–1561.
[73] S. Irrera, G. Portalone, First X-ray diffraction and quantum chemical study of proton-acceptor and proton-donor forms of 5-carboxylcytosine, the last-discovered nucleobase, J. Mol. Struct. 1050 (2013) 140–150.
[74] K. Ogawa, M. Kumihashi, K. Tomita, S. Shirotake, The structure of the cytosine-calcium chloride (1:1) complex. The first evidence for direct binding of calcium to cytosine base, Acta Crystallogr. B 36 (8) (1980) 1793–1797.
[75] G.M. Lombardo, G. Portalone, U. Chiacchio, A. Rescifina, F. Punzo, Potassium caffeate/caffeic acid co-crystal: the rat race between the catecholic and carboxylic moieties in an atypical co-crystal, Dalton Trans. 41 (2012) 14337–14344.
[76] J.P. Cleveland, B. Anczykowski, A.E. Schmid, V. Elings, Energy dissipation in tapping-mode atomic force microscopy, Appl. Phys. Lett. 72 (1998) 2613–2615.
[77] Z. Li, Y. Wang, A. Kozbial, G. Shenoy, F. Zhou, R. McGinley, P. Ireland, B. Morganstein, A. Kunkel, S.P. Surwade, L. Li, H. Liu, Effect of airborne contaminants on the wettability of supported graphene and graphite, Nat. Mater. 12 (2013) 925–934.
[78] D. Di Tommaso, E. Ruiz-Agudo, N.H. de Leeuw, A. Putnis, C.V. Putnis, Modelling the effects of salt solutions on the hydration of calcium ions, Phys. Chem. Chem. Phys. 16 (2014) 7772–7785.
[79] S. Santos, V. Barcons, H.K. Christenson, J. Font, N.H. Thomson, The intrinsic resolution limit in the atomic force microscope: implications for heights of nano-scale features, PLoS ONE 6 (2011) e23821.
[80] D. Passeri, M. Rossi, J.J. Vlassak, On the tip calibration for accurate modulus measurement by contact resonance atomic force microscopy, Ultramicroscopy 128 (2013) 32–41.
[81] L. Angeloni, D. Passeri, M. Reggente, D. Mantovani, M. Rossi, Removal of electrostatic artifacts in magnetic force microscopy by controlled magnetization of the tip: application to superparamagnetic nanoparticles, Sci. Rep. 6 (2016) 26293.
[82] L. Angeloni, D. Passeri, M. Reggente, M. Rossi, D. Mantovani, L. Lazzaro, F. Nepi, F. De Angelis, M. Barteri, Experimental issues in magnetic force microscopy of nanoparticles, AIP Conf. Proc. 1667 (2015) 020010.
[83] A.L. Weisenhorn, M. Khorsandi, S. Kasas, V. Gotzos, H.J. Butt, Deformation and height anomaly of soft surfaces studied with an AFM, Nanotechnology 4 (1993) 106–113.
[84] A. Knoll, R. Magerle, G. Kraush, Tapping mode atomic force microscopy on polymers: where is the true sample surface? Macromolecules 34 (2001) 4159–4165.
[85] X. Chen, M.C. Davies, C.J. Roberts, S.J.B. Tendler, P.M. Williams, J. Davies, A.C. Dawkes, J.C. Edwards, Interpretation of tapping mode atomic force microscopy data using amplitude-phase-distance measurements, Ultramicroscopy 75 (1998) 171–181.
[86] S. Kopp-Marsaudon, P. Leclère, F. Dubourg, R. Lazzaroni, J.P. Aimé, Quantitative measurement of the mechanical contribution to tapping-mode atomic force microscopy images of soft materials, Langmuir 16 (2000) 8432–8437.
[87] D. Passeri, M. Rossi, E. Tamburri, M.L. Terranova, Mechanical characterization of polymeric thin films by atomic force microscopy based techniques, Anal. Bioanal. Chem. 405 (2013) 1463–1478.
[88] E. Tamburri, S. Orlanducci, M.L. Terranova, F. Valentini, G. Palleschi, A. Curulli, F. Brunetti, D. Passeri, A. Alippi, M. Rossi, Modulation of the electrical properties in single-walled carbon nanotube/conducting polymer composites, Carbon 43 (2005) 1213–1221.
[89] D. Passeri, A. Alippi, A. Bettucci, M. Rossi, A. Alippi, E. Tamburri, M.L. Terranova, Indentation modulus and hardness of polyaniline thin films by atomic force microscopy, Synth. Met. 161 (2011) 7–12.
[90] D. Passeri, E. Tamburri, M.L. Terranova, M. Rossi, Polyaniline-nanodiamond fibers resulting from the self-assembly of nano-fibrils: a nanomechanical study, Nanoscale 7 (2015) 14358–14367.
[91] Q. Tu, B. Lange, Z. Parlak, J.M.J. Lopes, V. Blum, S. Zauscher, Quantitative subsurface atomic structure fingerprint for 2D materials and heterostructures by first-principles-calibrated contact-resonance atomic force microscopy, ACS Nano 10 (7) (2016) 6491–6500.
[92] D. Passeri, A. Bettucci, A. Biagioni, M. Rossi, A. Alippi, M. Lucci, I. Davoli, S. Berezina, Quantitative measurement of indentation hardness and modulus of compliant materials by atomic force microscopy, Rev. Sci. Instrum. 79 (2008) 066105.
[93] D. Passeri, A. Bettucci, A. Biagioni, M. Rossi, A. Alippi, E. Tamburri, M. Lucci, I. Davoli, S. Berezina, Indentation modulus and hardness of viscoelastic thin films by atomic force microscopy: a case study, Ultramicroscopy 109 (2009) 1417–1427.
[94] L.R.G. Treloar, Calculations of elastic moduli of polymer crystals: II. Terylene, Polymer 1 (1960) 279–289.
[95] K. Nakamae, T. Nishino, Y. Shimizu, T. Matsumoto, Experimental determination of the elastic modulus of crystalline regions of some aromatic polyamides, aromatic polyesters, and aromatic polyether ketone, Polym. J. 19 (1987) 451–459.
[96] J.R. Eskelsen, Y. Qi, S. Schneider-Pollack, S. Schmitt, K.W. Hipps, U. Mazur, Correlating elastic properties and molecular organization of an ionic organic nanostructure, Nanoscale 6 (2014) 316–327.
[97] K. Yamanaka, T. Tsuji, A. Noguchi, T. Koike, T. Mihara, Nanoscale elasticity measurement with in situ shape estimation in atomic force microscopy, Rev. Sci. Instrum. 71 (2000) 2403–2408.
[98] T. Tsuji, K. Yamanaka, Observation by ultrasonic atomic force microscopy of reversible displacement of subsurface dislocations in highly oriented pyrolytic graphite, Nanotechnology 12 (2001) 301–307.
[99] A. Richter, R. Ries, R. Smith, M. Henkel, B. Wolf, Nanoindentation of diamond, graphite and fullerene films, Diam. Relat. Mater. 9 (2000) 170–184.
[100] F. Gala, G. Zollo, Functionalization of hydrogenated (111) silicon surface with hydrophobic polymer chains, Phys. Rev. B 84 (2011) 195323.
[101] G. Ponti, F. Palombi, D. Abate, F. Ambrosino, G. Aprea, T. Bastianelli, F. Beone, R. Bertini, G. Bracco, M. Caporicci, B. Calosso, M. Chinnici, A. Colavincenzo, A. Cucurullo, P. Dangelo, M.D. Rosa, P.D. Michele, A. Funel, G. Furini, D. Giammattei, S. Giusepponi, R. Guadagni, G. Guarnieri, A. Italiano, S. Magagnino, A. Mariano, G. Mencuccini, C. Mercuri, S. Migliori, P. Ornelli, S. Pecoraro, A. Perozziello, S. Pierattini, S. Podda, F. Poggi, A. Quintiliani, A. Rocchi, C. Sciò, F. Simoni, A. Vita, The role of medium size facilities in the HPC ecosystem: the case of the new CRESCO4 cluster integrated in the ENEAGRID infrastructure, in: 2014 International Conference on High Performance Computing Simulation (HPCS), 2014, pp. 1030–1033.